Research Article

Interval type-II Takagi–Sugeno fuzzy-based strategy in control of autonomous systems

A. H. Mazinan[1]

Abstract
The present research addresses a new control strategy with a focus on an interval type-II Takagi–Sugeno (T–S) fuzzy-based approach in the area of autonomous systems to handle a set of parameters under model uncertainties. In a word, the subject behind the research is to guarantee the desirable performance of a class of the autonomous space robot systems through the design of the aforementioned interval type-II T–S fuzzy-based control strategy, which can be considered based upon the moments of inertia, the center of mass, the profile of the thrust vector and the misalignments of the propellant engine to deal with mission operation plans, in finite burning time. Concerning the research contribution, there are no solid foundations to address the investigated strategy to deal with such a system in the literatures, and therefore the proposed three-axis fuzzy-based comprehensive control solution, in its unique form, can be of the novelty, as long as a wide range of the mission operation plans are supported. It is to address a set of parameters of the autonomous space robot systems under model uncertainties, in a synchronous manner, while the outcomes are researched in connection with the specifications of the system under control and subsequently to be analyzed with regard to a number of benchmarks to verify the acquired performance. The key core behind the proposed research is to present a solving problem through the new integration of system control for a specific space autonomous task under control, while high-performance results in correspondence with the state-of-the-art materials are acquired.

Keywords Interval type-II Takagi–Sugeno fuzzy-based control strategy · Autonomous systems · Model uncertainties

1 Introduction

A fuzzy-based comprehensive control strategy is considered in the present research to handle the autonomous space robot systems that can be a challenging issue in this area to support mission operation plans by focusing on a wide range of the parameter variations. With this, the present research attempts to address an interval type-II Takagi–Sugeno (T–S) fuzzy-based control strategy to handle a class of overactuated autonomous space robot systems in some robotic maneuvers, in finite burning time, while the aforementioned parameters are varied based upon the model uncertainties with respect to time, in an abrupt manner. In the strategy proposed here, the on and off propellant engine modes are realized to be applicable in mission operation plans that are correspondingly related to autonomous space robot systems maneuvers through three control channels. In order to realize the strategy in these modes, the low-thrust three-axis engine off mode control approach, the low-thrust *x*-axis engine on mode control approach and also the high-thrust *y* and *z* axes engine on mode control approach are, respectively, designed to deal with a number of robotic maneuvers. It is to note that the engine on mode may be focused on the orbital maneuvers or other related attitude control cases, in finite burn time, which are encountering a band of uncertainties.

✉ A. H. Mazinan, mazinan@azad.ac.ir; ahmazinan@gmail.com; ah_mazinan@yahoo.com | [1]Department of Control Engineering, Faculty of Electrical Engineering, South Tehran Branch, Islamic Azad University (IAU), No. 209, NorthIranshahr St., P.O. Box 11365/4435, Tehran, Iran.

SN Applied Sciences (2019) 1:1393 | https://doi.org/10.1007/s42452-019-1425-0

Received: 6 April 2019 / Accepted: 9 October 2019 / Published online: 14 October 2019

And therefore, the corresponding engine off mode may be focused on the thermal, the communicational, the navigational, the specified attitude maneuvers and so on, in non-finite burn, respectively. Due to the fact that the uncertainties need to be addressed in engine on mode and these ones are not efficiently obvious in the corresponding engine off mode, the proposed interval type-II T–S fuzzy-based control strategy is only designed in the present research to deal with the same engine on mode. Moreover, there are a number of closed loops to be designed for the purpose of coping with the high–low-thrust three-axis control, in engine on mode, through two of them and the low-thrust three-axis control, in engine off mode, through the rest of them, as well. Now, to consider the contribution of the proposed control strategy, the backgrounds of the state-of-the-art materials in this area need to be first focused. Regarding the applicable state-of-the-art techniques, Sidi proposes some fundamental information in the area of space robot systems dynamics and its control [1]. Quadrelli describes an introduction of the space system dynamics and the corresponding control [2]. Zhou et al. consider the distributed cooperative control for finite-time attitude synchronization and also the coordination control for formation reconfiguration of multiple robotic systems [3, 4]. Yajie et al. address the uncertainty decomposition-based fault-tolerant adaptive control for the flexible ones, while Curran et al. discuss about the attitude control through the diamagnetic materials [5, 6]. Lee et al. propose finite-time control for body-fixed hovering over an asteroid and also Sun et al. discuss six degree-of-freedom integrated adaptive backstepping control for proximity operations [7, 8]. Eltantawie considers the decentralized neuro-fuzzy controllers of nonlinear quadruple tank system, where Hamzi et al. propose the kernel methods for the approximation of discrete-time linear autonomous and control systems [9, 10]. Rodriguez-Castaño et al. suggest the high-speed autonomous navigation system for heavy vehicles and Zhou et al. realize the observer-based controller for fuzzy systems with intermittent measurements [11, 12]. Da Sun et al. focus on the bilateral telerobotic system through type-II fuzzy neural network-based moving horizon estimation force observer for enhancement of environmental force compliance and human perception, while Taghavifar et al. deal with the path tracking of autonomous vehicles via an adaptive robust exponential-like sliding-mode fuzzy type-II neural network controller [13, 14]. Ghobaei-Arani et al. cope with the autonomous resource provisioning framework for massive multiplayer online games in cloud environment, as long as Lughofer et al. explore the autonomous supervision and optimization of product quality in a multistage manufacturing process based on self-adaptive prediction models [15, 16]. Furthermore, Lughofer et al. work on the self-adaptive evolving forecast models with incremental space updating for online prediction of micro-fluidic chip quality, where Gaidhane et al. design the interval type-II fuzzy pre-compensated controller applied to robotic manipulator with variable payload [17, 18]. Onieva et al. suggest the multi-objective evolutionary algorithm for the tuning of fuzzy rule bases for uncoordinated intersections in autonomous driving, and Cordón proposes the historical review of evolutionary learning methods for Mamdani-type fuzzy rule-based systems by designing interpretable genetic fuzzy systems [19, 20]. Igor Škrjanc et al. survey the evolving fuzzy and neuro-fuzzy approaches in clustering, regression, identification, and classification, while Sinan özbek et al. design the optimal fractional fuzzy gain-scheduled predictor for a time-delay process with experimental application [21, 22]. Engin Yesil presents the interval type-II fuzzy load frequency controller using optimization method, Sharina Huang et al. construct the optimized interval type-II neuro-fuzzy systems with noise reduction property, and finally, Meza-Sánchez et al. investigate the synthetic–analytic behavior-based control framework by constraining velocity in tracking for nonholonomic wheeled mobile robots [23–25]. The key core of finding the new outcomes in the approach presented here is to realize a unique three-channel comprehensive control strategy that is able to deal with a class of the autonomous space robot systems under control with efficient results, as long as the variations of a set of parameters are not able to avoid guaranteeing the appropriate performance with high accuracy with respect to the potential investigations in this area. It is to note that the proposed research is focused on solving problem by proposing the new integration of system control for a specific space autonomous task under control with high-performance results in line with the state-of-the-art materials.

The rest of the manuscript is organized as follows: The proposed control strategy including preliminary materials and the overall strategy realization are first presented in Sect. 2, while the simulation results and concluding remarks are then presented in Sects. 3 and 4, respectively.

2 The proposed control strategy

The realization of the overall strategy is presented along with the integration of so many employed modules, as shown in Fig. 1, to be applicable to handle a class of autonomous robotic systems. It means that the specifications of the same class of the autonomous space robot systems should be related to the moments of inertia, the center of mass concerning the overall autonomous robotic system and also the profiles of the thrust vector, the misalignments concerning the propellant engine of

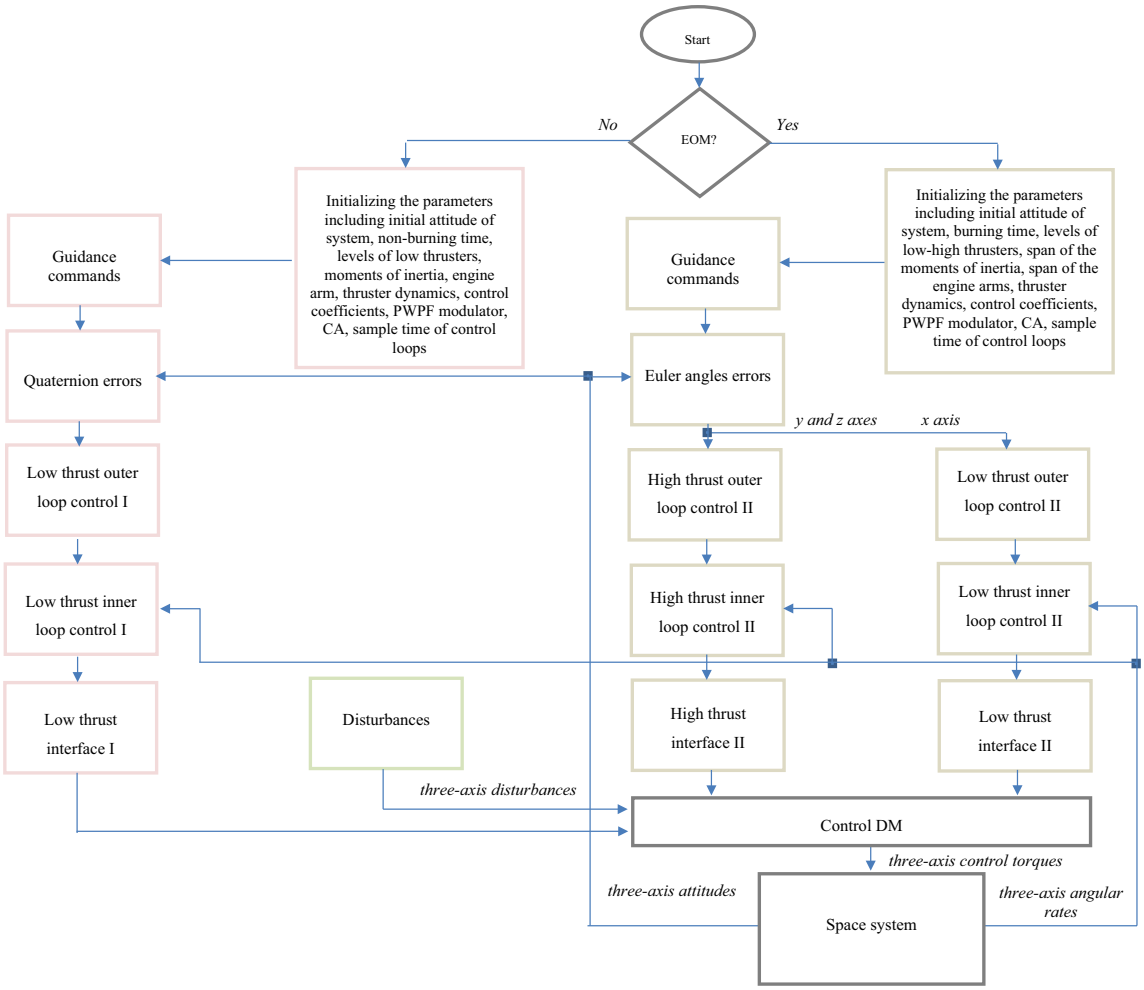

Fig. 1 Proposed control strategy

the same autonomous robotic system. Now, to follow the investigated outcomes, at first, the specific mode of propellant engine has to be identified through engine on mode (EOM) conditional block. As are apparent, each one of the modes needs to be dealt with in the three axes. With this purpose, the realizations of the control approaches are considered in the three separated channels including the low-thrust three-axis control approach I to be designed in the engine off mode and also the low- and high-thrust three-axis control approach II to be designed in engine on mode, respectively. It is obvious that the procedures of realizing them are different, due to the fact that their applicabilities are not the same, surely. The investigated outcomes concerning these control approaches are given in the proceeding subsections.

2.1 The low-thrust three-axis control approach I

The low-thrust three-axis control approach I is shown in Fig. 1. There are also the low-thrust interface module to provide the three-axis control torques of the system under control based on the definition of the pulse-width pulse frequencies (PWPFs) with the parameters of k, τ and $U_{\text{on,off}}$ as the gain, time constant and hysteresis, respectively, and also the control allocations (CAs) with the parameters of α and β as the radius of the thruster's configuration and the engine arm, respectively, to deal with a number of reaction thrusters by Eq. (1)

$$\text{CA}_{ml1} = \begin{bmatrix} 0 & 0 & 0 & 0 & -\alpha & -\alpha & \alpha & \alpha \\ -\alpha & 0 & \alpha & 0 & 0 & \beta & 0 & -\beta \\ 0 & \alpha & 0 & -\alpha & \beta & 0 & -\beta & 0 \end{bmatrix} \tag{1}$$

The general materials of such aforementioned modules are not reported and are easily available to use [3]. A number of parameters need to be first initialized such as initial attitude of system, non-burning time, levels of low thrusters, moments of inertia, engine arm and thruster dynamics with the parameters of k_t, τ_t and d_t as the gain, time

constant and delay, respectively, in the form of $\frac{k_t}{1+\tau_t s}e^{-d_t s}$. And there are control coefficients, PWPFs, CAs, sample time of control loops to be all programmed. Now, the three-axis efforts of the aforementioned control approach are provided by Eq. (2)

$$\begin{pmatrix}\tau_x\\ \tau_y\\ \tau_z\end{pmatrix}=\begin{pmatrix}-T\left(k_{px}q_{1e}+k_{dx}\omega_x\right)\\ -T\left(k_{py}q_{2e}+k_{dy}\omega_y\right)\\ -T\left(k_{pz}q_{3e}+k_{dz}\omega_z\right)\end{pmatrix} \tag{2}$$

where by using $\boldsymbol{q_e}=\boldsymbol{q_{\mathrm{ref}}}\boldsymbol{q_s}$, its expanded form is written by Eq. (3)

$$\begin{bmatrix}q_{1e}\\ q_{2e}\\ q_{3e}\\ q_{4e}\end{bmatrix}=\begin{bmatrix}q_{4\mathrm{ref}} & q_{3\mathrm{ref}} & -q_{2\mathrm{ref}} & -q_{1\mathrm{ref}}\\ -q_{3\mathrm{ref}} & q_{4\mathrm{ref}} & q_{1\mathrm{ref}} & -q_{2\mathrm{ref}}\\ q_{2\mathrm{ref}} & -q_{1\mathrm{ref}} & q_{4\mathrm{ref}} & -q_{3\mathrm{ref}}\\ q_{1\mathrm{ref}} & q_{2\mathrm{ref}} & q_{3\mathrm{ref}} & q_{4\mathrm{ref}}\end{bmatrix}\begin{bmatrix}q_{1s}\\ q_{2s}\\ q_{3s}\\ q_{4s}\end{bmatrix} \tag{3}$$

In one such case, the thrust's level T is the same for all the thrusters and also the conditions $\| \boldsymbol{q_{\mathrm{ref}}} \| = 1$ must be satisfied. In this formulation, $\boldsymbol{q_e}$ is taken as quaternion error, and $\boldsymbol{q_s}$ is taken as system quaternion, and finally $\boldsymbol{q_{\mathrm{ref}}}$ is taken as referenced quaternion.

2.2 The low- and high-thrust three-axis control approach II

Regarding the low- and high-thrust three-axis control approach II, the procedure of realizing this is shown in Fig. 1. And there are thruster's dynamics, PWPFs and CAs with the same definitions of the parameters of the previous control approach, in which the aforementioned CAs should be programmed by Eq. (4)

$$\mathrm{CA}_{ml2}=\begin{bmatrix}-\alpha & -\alpha & \alpha & \alpha\end{bmatrix},\ \mathrm{CA}_{mh2}=\begin{bmatrix}0 & -\alpha & 0 & \alpha\\ \alpha & 0 & -\alpha & 0\end{bmatrix} \tag{4}$$

With this procedure, it is certainly possible to organize the whole of x, y and z axes in high thrust, although the tracking of the x-axis of the autonomous robotic system via the control strategy proposed here plays insignificant role to guarantee the system performance with regard to the tracking of the both y and z referenced commands, correspondingly. These three-axis disturbances are generated through the profiles of the thrust vector ($\boldsymbol{F}$), engine misalignments $\left(\varphi_{\mathrm{mis}},\theta_{\mathrm{mis}},\psi_{\mathrm{mis}}\right)$ and engine arm ($\boldsymbol{r}$) to be updated by the variation of the center of mass $\left(\Delta\boldsymbol{c_g}\right)$, as input sources, inspired of Eq. (5)

$$\boldsymbol{\tau_{\mathrm{dis}}}=\boldsymbol{L}\times\boldsymbol{F}\,\mathrm{DCM}\left(\varphi_{\mathrm{mis}},\theta_{\mathrm{mis}},\psi_{\mathrm{mis}}\right) \tag{5}$$

The outcomes are finalized, where the matrix multiplication of the direction cosine matrix (DCM) of the misalignments profile can be multiplied in cross-form by $\boldsymbol{L}=\boldsymbol{r}+\Delta\boldsymbol{c_g}$ deviation profile, at each instant of time. The idea of the proposed interval type-II T–S fuzzy-based control approach is realized in the low- and high-thrust control approach, described in the proceeding subsection.

2.2.1 The interval type-II fuzzy-based control approach

The interval type-II fuzzy-based control approach is designed in this research to handle the low- and high-thrust three-axis control approach II. The key idea of the present fuzzy-based control approach is now briefly demonstrated. The present approach consists of fuzzifier, rule base, inference engine and defuzzifier with type reducer. The present approach is described through type-II membership function, i.e., $\mu_{\tilde{X}}(x,u)$ by Eq. (6)

$$\tilde{X}=\int_{x\,\epsilon\,D_{\tilde{x}}}\int_{u\,\epsilon\,J_x}\frac{\mu_{\tilde{X}}(x,u)}{(x,u)} \tag{6}$$

where $\iint$ indicates the union over x and u and also $J_x\subseteq[0,1]$ is related to the primary membership function of x in case of $\mu_{\tilde{X}}(x,u)$ that is the type-I fuzzy-based approach known as the secondary set [1, 2].

It should be noted that the uncertainties in the primary membership of the type-II fuzzy set $\tilde{X}$ is described by a region entitled to the footprint of uncertainty, (FOU) that can be presented based on the upper membership function (UMF) $\bar{\mu}_{\tilde{X}}$ and the lower membership function (LMF) $\underline{\mu}_{\tilde{X}}$. In this regard, the schematic diagram of the interval type-II fuzzy-based approach is shown in Fig. 2. The T–S type of the aforementioned interval type-II fuzzy-based control approach is designed by $l=1,2,\ldots,M$ rules as given in Eq. (7):

$$\mathrm{Rule}^l:\ \text{If } x_1 \text{ is } \tilde{X}_1^l \text{ and } x_2 \text{ is } \tilde{X}_2^l \text{ and } \ldots \text{ and } x_n \text{ is } \tilde{X}_n^l \text{ Then } y \text{ is } Y^l \tag{7}$$

where $\tilde{X}_i^l; i=1,2,\ldots,n$ are taken as the antecedent membership functions, and $Y^l=\left[\underline{y}^l,\bar{y}^l\right]$ are also taken as the consequent membership functions regarding the interval type-II fuzzy-based approach. In this way, $\underline{y}^l$ and $\bar{y}^l$ are the crisp consequent of the linear function, presented by Eq. (8):

$$\begin{cases}\underline{y}^l=\underline{b}^l+\sum_{i=1}^{l}\underline{a}_i^l x_i\\ \bar{y}^l=\bar{b}^l+\sum_{i=1}^{M}\bar{a}_i^l x_i\end{cases} \tag{8}$$

By using the crisp input vector, i.e., $x'=\left[x_1',x_2',\ldots,x_n'\right]$, the interval membership of x_i' regarding the

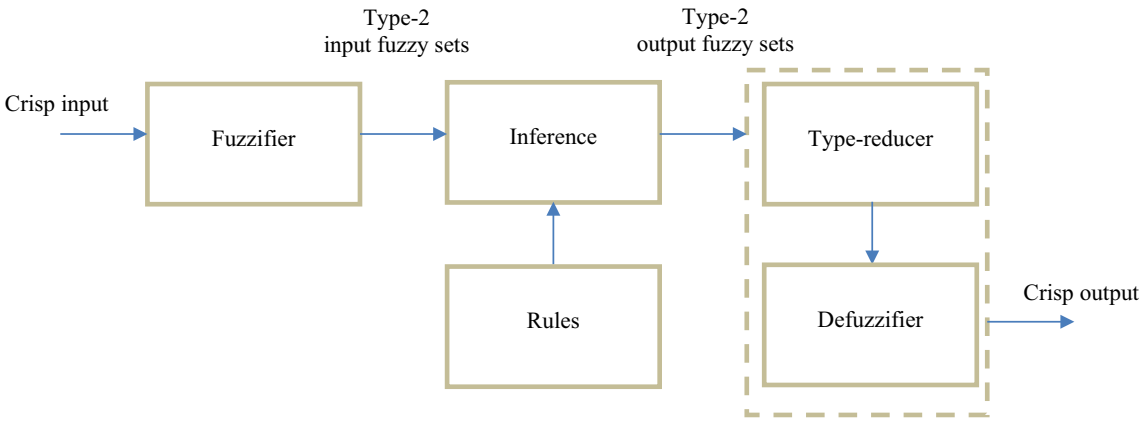

Fig. 2 Type-II fuzzy-based system

$\tilde{X}_i^l, [\mu_{\underline{\tilde{X}}_i^l}(x_i'), \bar{\mu}_{\tilde{X}_i^l}(x_i')], i = 1, 2, \ldots, n; l = 1, 2, \ldots, M$ is taken. Now, the rule firing interval of the $F^l(x') = \left[\underline{f}^l, \bar{f}^l\right]$ can be calculated, while $\underline{f}^l = \left[\mu_{\underline{\tilde{X}}_1^l}(x_1') * \mu_{\underline{\tilde{X}}_2^l}(x_2') * \ldots * \mu_{\underline{\tilde{X}}_n^l}(x_n')\right]$ and $\bar{f}^l = \left[\bar{\mu}_{\tilde{X}_1^l}(x_1') * \bar{\mu}_{\tilde{X}_2^l}(x_2') * \ldots * \bar{\mu}_{\tilde{X}_n^l}(x_n')\right]$ are denoted. By applying the type reduction process to provide $F^l(x')$ and the corresponding rule consequents, the y_q and y_r are presented as Eq. (9):

$$\begin{cases} y_q = \frac{\sum_{l=1}^{Q} \underline{y}^l \bar{f}^l + \sum_{l=Q+1}^{M} \underline{y}^l \underline{f}^l}{\sum_{l=1}^{Q} \bar{f}^l + \sum_{l=Q+1}^{M} \underline{f}^l} \\ y_r = \frac{\sum_{l=1}^{R} \bar{y}^l \underline{f}^l + \sum_{l=R+1}^{M} \bar{y}^l \bar{f}^l}{\sum_{l=1}^{R} \underline{f}^l + \sum_{l=R+1}^{M} \bar{f}^l} \end{cases} \tag{9}$$

where Q and R are taken as the switching points, and also there is the center of set (COS) type reducer defined as Eq. (10):

$$Y_{\cos}(x') = \bigcup \frac{\sum_{l=1}^{M} y^l f^l}{\sum_{l=1}^{M} f^l} = [y_q, y_r] \tag{10}$$

Finally, the crisp output is calculated as Eq. (11)

$$y = \frac{y_q + y_r}{2} \tag{11}$$

3 The simulation results

In order to analyze the applicability of the strategy proposed here, at first, two separated experiments regarding the low-thrust three-axis control approach I to address the engine off mode (Exp*#1*) and also the low- and high-thrust three-axis control approach II to address the engine on mode (Exp*#2*) are organized to be considered. The specifications of the autonomous robotic system is presented along with the parameters including the moments of inertia, the center of mass, the profile of the thrust vector and the misalignments of the propellant engine, where the variations are notable in engine on mode with respect to the corresponding engine off mode. The three-axis engine arm is initially taken as $[-0.8, 0, 0]^T(m)$. In one such case, the initial parameters, in engine off mode, are tabulated in Table 1.

Moreover, the initial parameters, in engine on mode, are tabulated in Table 2.

The control solutions of the low- and high-thrust three-axis control approach II, in engine on mode, is first realized based upon the interval type-II T–S fuzzy-based control approach with regard to the proportional–integral–derivative method, while the following lower and upper antecedent Gaussian membership functions, which are presented by the parameters of σ and m in the form of $e^{-\frac{(x-m)^2}{2\sigma^2}}$, respectively, are taken to address the whole of inputs variables including the errors ((In^1), the derivative of errors ((In^2) and the integral of errors In^3, synchronously, in the three axes.

$$\begin{cases} M_f l^1 = [4.58e-2 \quad -1.50e-1] \\ M_f u^1 = [5.09e-2 \quad -1.50e-1] \\ M_f l^2 = [4.58e-2 \quad 0] \\ M_f u^2 = [5.09e-2 \quad 0] \\ M_f l^3 = [4.58e-2 \quad 1.50e-1] \\ M_f u^3 = [5.09e-2 \quad 1.50e-1] \end{cases} \tag{12}$$

Subsequently, there are three crisp consequent membership functions in the form of linear for output to be taken to deal with the *x*-axis control approach.

Table 1 In case of experiment 1, the initial parameters of the proposed low-thrust three-axis control approach I, in engine off mode

	Parameters	Values
1	The number of low thrusters	8
2	Low thruster's level	$T_L = 15$
3	Low-thrust three-axis control coefficients in the outer loop	$\begin{cases} k_{pxyz} = 72 \\ k_{dxyz} = 200 \\ k_{ixyz} = 0 \end{cases}$
4	Low-thrust three-axis control coefficients in the inner loop	$k_{pxyz} = 15$
5	Low-thrust three-axis PWPF coefficients	$\begin{cases} K_{xyz} = 5 \\ \tau_x = 0.35 \\ \tau_{yz} = 0.50 \\ U_{onxyz} = 0.80 \\ U_{offxyz} = 0.10 \end{cases}$
6	Moments of inertia	$\begin{cases} I_x = 30 \\ I_y = 45 \\ I_z = 48 \end{cases}$
7	CAs coefficients	$\begin{cases} \alpha = 0.5 \\ \beta = -0.8 : -0.5 \end{cases}$
8	Thruster's dynamics	$\begin{cases} k_t = 1 \\ \tau_t = 0.01 \\ d_t = 0.01 \end{cases}$
9	Sampling time	0.01
10	Non-burning time (s)	500

Table 2 In case of experiment 2, the initial parameters of the proposed control strategy II, in engine off mode

	Parameters	Values
1	The number of low thrusters	4
2	The number of high thrusters	4
3	Low thruster's level	$T_L = 150$
4	High thruster's level	$T_H = 600$
5	High- and low-thrust three-axis PWPF coefficients	$\begin{cases} K_{xyz} = 55 \\ \tau_{xyz} = 0.0075 \\ U_{on} = 0.80 \\ U_{off} = 0.10 \end{cases}$
6	Moments of inertia	$\begin{cases} I_x = 30 : 26 \\ I_y = 45 : 39 \\ I_z = 48 : 42 \end{cases}$
7	CAs coefficients	$\alpha = 0.5$
8	Thruster's dynamics	$\begin{cases} k_t = 1 \\ \tau_t = 0.01 \\ d_t = 0.03 \end{cases}$
9	Sampling time	0.01
10	Burning time (s)	200

Table 3 In case of experiment 2, the fuzzy rules in case of In^3 is $\tilde{M}_f^1$ for the low- and high-thrust three-axis control approach II

In^1/In^2	$\tilde{M}_f^1$	$\tilde{M}_f^2$	$\tilde{M}_f^3$
$\tilde{M}_f^1$	M_f^1	M_f^1	M_f^1
$\tilde{M}_f^2$	M_f^1	M_f^2	M_f^2
$\tilde{M}_f^3$	M_f^1	M_f^3	M_f^3

Table 4 In case of experiment 2, the fuzzy rules in case of In^3 is $\tilde{M}_f^2$ for the low- and high-thrust three-axis control approach II

In^1/In^2	$\tilde{M}_f^1$	$\tilde{M}_f^2$	$\tilde{M}_f^3$
$\tilde{M}_f^1$	M_f^1	M_f^2	M_f^1
$\tilde{M}_f^2$	M_f^2	M_f^2	M_f^2
$\tilde{M}_f^3$	M_f^3	M_f^2	M_f^3

Table 5 In case of experiment 2, the fuzzy rules in case of In^3 is $\tilde{M}_f^3$ for the low- and high-thrust three-axis control approach II

In^1/In^2	$\tilde{M}_f^1$	$\tilde{M}_f^2$	$\tilde{M}_f^3$
$\tilde{M}_f^1$	M_f^1	M_f^1	M_f^3
$\tilde{M}_f^2$	M_f^2	M_f^2	M_f^3
$\tilde{M}_f^3$	M_f^3	M_f^3	M_f^3

$$\begin{cases} M_f^1 = [\,4.873e2 \;\; 2.883e3 \;\; 1.100.0e3 \;\; 0\,] \\ M_f^2 = \left[\,4.430e2 \;\; 2.621e3 \;\; 1.000e3 \;\; 0\,\right] \\ M_f^3 = \left[\,3.987e2 \;\; 2.359e3 \;\; 9.000e2 \;\; 0\,\right] \end{cases} \tag{13}$$

And the same crisp consequent membership functions for *y* and *z* axes are, respectively, taken by

$$\begin{cases} M_f^1 = [2.015e4 \quad 0 \quad 1.735e4 \quad 0] \\ M_f^2 = [1.832e3 \quad 0 \quad 1.577e4 \quad 0] \\ M_f^3 = [1.649e3 \quad 0 \quad 1.419e3 \quad 0] \end{cases} \tag{14}$$

$$\begin{cases} M_f^1 = [3.282e4 \quad 0 \quad 9.832e3 \quad 0] \\ M_f^2 = [2.984e4 \quad 0 \quad 8.938e3 \quad 0] \\ M_f^3 = [2.686e4 \quad 0 \quad 8.044e3 \quad 0] \end{cases} \tag{15}$$

These outcomes regarding the aforementioned three-axis membership functions presented here are all taken as the extended ones of realizing the proportional–integral–derivative control approach, while its optimum coefficients are correspondingly acquired through MATLAB optimization toolbox. Now, it should be also noted that the fuzzy rules, which are used in the proposed interval type-II T–S fuzzy-based control approach for *x*, *y* and *z* axes, are separately tabulated in Tables 3, 4 and 5.

Regarding the experiment, the referenced commands are taken as $\varphi_{\text{ref}} = 0°, \theta_{\text{ref}} = -55°$ and $\psi = 105°$ in the span of $0 - 200$ s, where the corresponding initial values are taken as $\varphi_{\text{ref0}} = 0°, \theta_{\text{ref0}} = -58°$ and $\psi_{\text{ref0}} = 120°$,

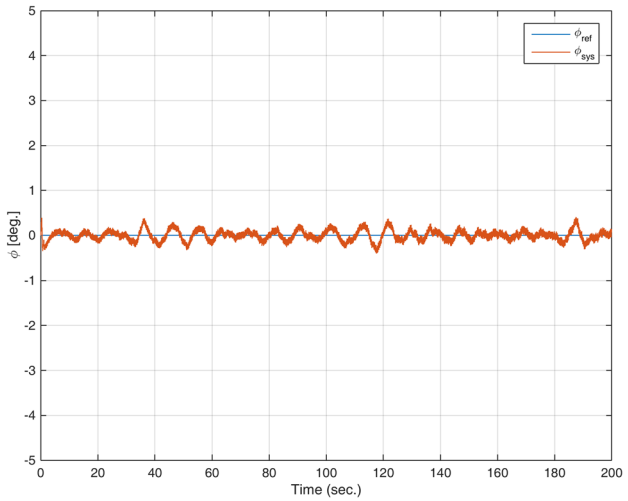

Fig. 3 Results for the *x*-axis referenced command tracking

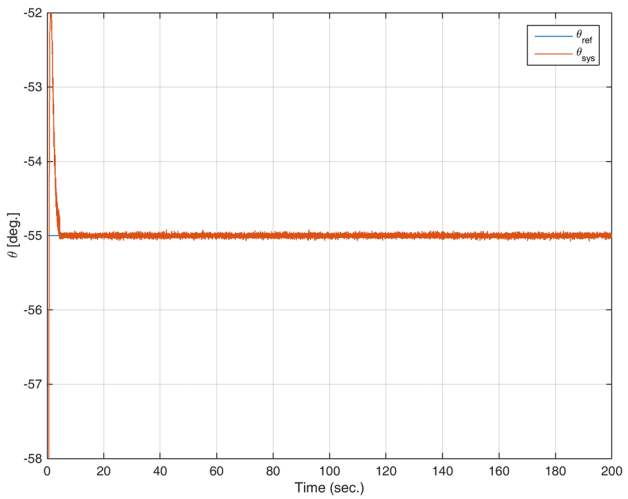

Fig. 4 Results for the *y*-axis referenced command tracking

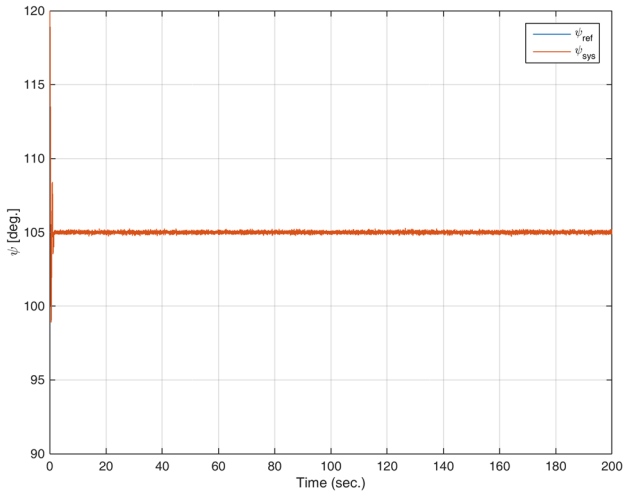

Fig. 5 Results for the *z*-axis referenced command tracking

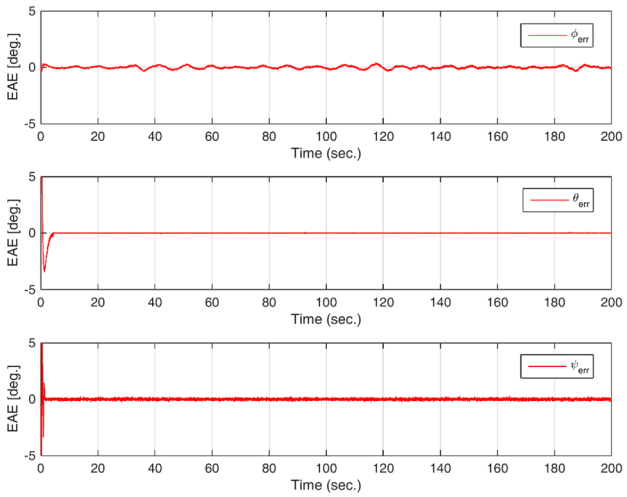

Fig. 6 Three-axis referenced commands tracking errors

respectively. The tracking outcomes of the present referenced commands are averagely calculated after a number of iterations with model uncertainties, where the outcomes concerning the worst case are shown in Figs. 3, 4, 5, respectively. Correspondingly, the three-axis tracking errors of the referenced commands are given in Fig. 6. The results indicate that the control approach proposed here is able to deal with the system under control in the provided referenced commands considering the initial parameters of system.

3.1 The control strategy performance verification

The performance of the proposed control strategy is considered to be verified through the interval type-II T–S fuzzy-based control approach with regard to the proportional–integral–derivative method (Case I) in connection with the type-I fuzzy-based control approach with regard to the proportional–integral–derivative method (Case II) and also the traditional proportional–integral–derivative control approach (Case III) through the calculations of the integral square error (ISE), the integral time square error (ITSE), the integral absolute error (IAE) and finally the integral time absolute error (ITAE) as

Table 6 Control strategy performance verification in some cases

		ISE_x	ISE_y	ISE_z	$ITSE_x$	$ITSE_y$	$ITSE_z$	IAE_x	IAE_y	IAE_z	$ITAE_x$	$ITAE_y$	$ITAE_z$
1	Case I	2.992	0.0760	0.934	292.9	7.613	93.72	19.48	3.853	13.52	1923	385.5	1354
2	Case II	5.564	1.507	6.941	544.7	151.10	699.2	26.57	16.31	36.04	2622	1634	3623
3	Case III	673.2	79.17	97.20	65,910	576.5	5035	292.3	37.37	90.55	28,840	2822	8852

$$\begin{cases} \mathrm{ISE} = \int_0^\infty e^2(t)\mathrm{d}t \\ \mathrm{ITSE} = \int_0^\infty te^2(t)\mathrm{d}t \\ \mathrm{IAE} = \int_0^\infty |e(t)|\mathrm{d}t \\ \mathrm{ITAE} = \int_0^\infty t|e(t)|\mathrm{d}t \end{cases} \tag{16}$$

For all the considered cases, the specifications of the system under control are the same as in Table 2, and also the uncertainties through a set of mentioned parameters variations are taken as Exp#2, throughout the experiments to be totally comparable. The realization of the Case I is considered based on the information presented in Eqs. (12)–(15) and the results tabulated in Tables 3, 4 and 5, as well.

Moreover, the realization of the Case II is considered as the concise form of the Case I by eliminating the FOU. With this goal, the antecedent Gaussian membership functions with the same definition of the parameters of σ and m,respectively, are taken to address the inputs variables, in the three axes, by the following, while the consequence membership functions and rules base are the same as the Case I.

$$\begin{cases} \tilde{M}_f^1 = M_f^1 = [5.09e-2 \quad -1.50e-1] \\ \tilde{M}_f^2 = M_f^2 = [5.60e-2 \quad 0] \\ \tilde{M}_f^3 = M_f^3 = [5.60e-2 \quad 1.50e-1] \end{cases} \tag{17}$$

Finally, the realization of the Case III, in the three axes, is given based on the MATLAB optimization toolbox, while the acquired coefficients are resulted by the following:

$$\begin{cases} \mathrm{Coeff\_}x = \begin{bmatrix} 4.430e2 & 2.621e3 & 1.000e3 \end{bmatrix} \\ \mathrm{Coeff\_}y = \begin{bmatrix} 1.832e3 & 0 & 1.577e4 \end{bmatrix} \\ \mathrm{Coeff\_}z = \begin{bmatrix} 2.984e4 & 0 & 8.938e3 \end{bmatrix} \end{cases} \tag{18}$$

Now, the investigated three-axis results are correspondingly tabulated in Table 6.

Subsequently, the results indicate that the proposed interval type-II T–S fuzzy-based control approach with regard to the proportional–integral–derivative method is well-behaved based on the investigated results in case of the type-I fuzzy-based control approach with regard to the proportional–integral–derivative method and also the traditional proportional–integral–derivative control approach to deal with the system under control.

4 Conclusion

The present research attempts to address an interval type-II Takagi–Sugeno fuzzy-based control strategy with a focus on a set of parameters of the system under control with model uncertainties, while the desirable performance is guaranteed. There are a realization of the aforementioned control strategy to deal with the present system in engine off mode, which are organized based upon the technique of quaternion and also in engine off mode to deal with moments of inertia, the central of mass, the profile of the thrust vector and the misalignments of the propellant engine to deal with mission operation plans. It should be noted that the discussion on solving problem in this research is to propose the new integration of system control with a focus on a specific space autonomous task with high-performance outcomes with respect to the state-of-the-art materials.

Compliance with ethical standards

Conflict of interest The corresponding author states that there is no conflict of interest.

References

1. Sidi MJ (1997) Spacecraft dynamics and control. Aircraft Industries Ltd. and Aviv University, Tel Aviv
2. Karunarathne D, Morales Y, Kanda T, Ishiguro H (2018) Model of side-by-side walking without the robot knowing the goal. Int J Soc Robot 10(4):401–420
3. Zhou N, Xia Y, Fu M, Li Y (2015) Distributed cooperative control design for finite-time attitude synchronisation of rigid spacecraft. IET Control Theory Appl 9(10):1561–1570
4. Zhou N, Xia Y (2015) Coordination control design for formation reconfiguration of multiple spacecraft. IET Control Theory Appl 9(15):2222–2231
5. Ma Y, Jiang B, Tao G, Cheng Y (2015) Uncertainty decomposition-based fault-tolerant adaptive control of flexible spacecraft. IEEE Trans Aerosp Electron Syst 51(2):1053–1068

6. Curran J, Hussman C (2015) Pioneering the application of diamagnetic materials for spacecraft attitude control. IEEE Commun Mag 53(5):200–201
7. Lee D, Sanyal AK, Butcher EA, Scheeres DJ (2015) Finite-time control for spacecraft body-fixed hovering over an asteroid. IEEE Trans Aerosp Electron Syst 51(1):506–520
8. Sun L, Huo W (2015) 6-DOF integrated adaptive backstepping control for spacecraft proximity operations. IEEE Trans Aerosp Electron Syst 51(3):2433–2443
9. Eltantawie MA (2019) Decentralized neuro-fuzzy controllers of nonlinear quadruple tank system. SN Appl Sci 1:39
10. Hamzi B, Colonius F (2019) Kernel methods for the approximation of discrete-time linear autonomous and control systems. SN Appl Sci 1:674
11. Rodriguez-Castaño A, Heredia G, Ollero A (2016) High-speed autonomous navigation system for heavy vehicles. Appl Soft Comput 43:572–582
12. Zhou Q, Liu D, Sun K, Wu C, Xing X (2016) Design of observer-based controller for T–S fuzzy systems with intermittent measurements. Neurocomputing 174(Part B):689–697
13. Sun D, Liao Q, Stoyanov T, Kiselev A, Loutfi A (2019) Bilateral telerobotic system using type-2 fuzzy neural network based moving horizon estimation force observer for enhancement of environmental force compliance and human perception. Automatica 106:358–373
14. Taghavifar H, Rakheja S (2019) Path-tracking of autonomous vehicles using a novel adaptive robust exponential-like-sliding-mode fuzzy type-2 neural network controller. Mech Syst Signal Process 130:41–55
15. Ghobaei-Arani M, Khorsand R, Ramezanpour M (2019) An autonomous resource provisioning framework for massively multiplayer online games in cloud environment. J Netw Comput Appl 142:76–97
16. Lughofer E, Zavoianu AC, Pollak R, Pratama M, Radauer T (2019) Autonomous supervision and optimization of product quality in a multi-stage manufacturing process based on self-adaptive prediction models. J Process Control 76:27–45
17. Lughofer E, Pollak R, Zavoianu AC, Pratama M, Radauer T (2018) Self-adaptive evolving forecast models with incremental PLS space updating for on-line prediction of micro-fluidic chip quality. Eng Appl Artif Intell 68:131–151
18. Gaidhane PJ, Nigam MJ, Kumar A, Pradhan PM (2019) Design of interval type-2 fuzzy precompensated PID controller applied to two-DOF robotic manipulator with variable payload. ISA Trans 89:169–185
19. Onieva E, Hernandez-Jayo U, Osaba E, Perallos A, Zhang X (2015) A multi-objective evolutionary algorithm for the tuning of fuzzy rule bases for uncoordinated intersections in autonomous driving. Inf Sci 321:14–30
20. Cordón O (2011) A historical review of evolutionary learning methods for Mamdani-type fuzzy rule-based systems: designing interpretable genetic fuzzy systems. Int J Approx Reason 52(6):894–913
21. Škrjanc I, Iglesias JA, Sanchis A, Leite D, Gomide F (2019) Evolving fuzzy and neuro-fuzzy approaches in clustering, regression, identification, and classification: a survey. Inf Sci 490:344–368
22. özbek NS, Eker I (2019) Design of an optimal fractional fuzzy gain-scheduled Smith Predictor for a time-delay process with experimental application. ISA Trans, in press, August 2019
23. Yesil Engin (2014) Interval type-2 fuzzy PID load frequency controller using Big Bang-Big Crunch optimization. Appl Soft Comput 15:100–112
24. Huang S, Chen M (2016) Constructing optimized interval type-2 TSK neuro-fuzzy systems with noise reduction property by quantum inspired BFA. Neurocomputing 173(Part 3):1839–1850
25. Meza-Sánchez M, Clemente E, Rodríguez-Liñán MC, Olague G (2019) Synthetic-analytic behavior-based control framework: constraining velocity in tracking for nonholonomic wheeled mobile robots. Inf Sci 501:436–459